On the dynamics of an idealised bottom density current overflowing in a semi-enclosed basin: mesoscale and submesoscale eddies generation

Mathieu Morvan, Xavier Carton, Pierre L'Hégaret, Charly de Marez, Stéphanie Corréard, Stéphanie Louazel

Geophysical And Astrophysical Fluid Dynamics
September 2020, Volume 114 Issue 4-5 Pages 607-630
https://doi.org/10.1080/03091929.2020.1747058
https://archimer.ifremer.fr/doc/00627/73918/

On the dynamics of an idealised bottom density current overflowing in a semi-enclosed basin: mesoscale and submesoscale eddies generation

Morvan Mathieu [1, *], Carton Xavier [1], L'Hégaret Pierre [1], De Marez Charly [1], Corréard Stéphanie [2], Louazel Stephanie [3]

[1] LOPS, Univ. Brest-CNRS-IFREMER-IRD, IUEM, Plouzané, France
[2] SHOM/DOPS/STM/DTO, Toulouse Cedex 5, France
[3] SHOM/DOPS/STM/DTO, Brest Cedex 2, France

* Corresponding author : Mathieu Morvan, email address : mmorvan3@univ-brest.fr

Abstract :

The Red Sea Water enters the Gulf of Aden through the Strait of Bab El Mandeb as a density current. The Red Sea Water subsequently spreads into the Gulf of Aden under the influence of surface mesoscale eddies, which dominate the surface flow, of topographic features such as rift and capes, and of the monsoon regimes. The dynamics of a bottom density current overflowing in a semi-enclosed basin, as the Red Sea Water outflows in the Gulf of Aden, is investigated by performing idealised numerical simulations, at submesoscale resolution, in which we progressively add topographic and dynamical elements. The rift and cape play an important role, respectively, on the vertical and the horizontal mixing as well as baroclinic and barotropic instabilities undergone by the bottom density current. Mesoscale and submesoscale eddies are generated depending on the model configuration. In the presence of surface mesoscale eddies, the bottom density current water is mainly advected at their periphery. In winter, both mesoscale and submesoscale eddies are generated, while in summer only submesoscale eddies are present. Finally, to put our results based on idealised numerical simulations and Lagrangian experiments in perspective, we analyse the trajectories of three Argo floats, deployed in the Rift of Tadjurah. Clues of submesoscale eddies generation at capes are observed which is in agreement with our idealised numerical simulations.

Keywords : Bottom density current, Red Sea outflow, submesoscale eddies, current instability, mesoscale eddies

1. Introduction

The Red Sea is a marginal sea connected to the Arabian Sea *via* the Strait of Bab El Mandeb and the Gulf of Aden. The Red Sea Water (RSW) is a warm and salty (dense) water formed in the Red Sea due to strong evaporation there, as well as negligible precipitation (Bower *et al.* 2000). The RSW enters the Gulf of Aden throughout the Strait of Bab El Mandeb as a density current. *In situ* measurements have shown the seasonal variability of the RSW transport at the Strait of Bab El Mandeb (Murray and Johns 1997), due to the monsoon winds. The temperature and salinity of RSW are respectively equal to 22.9 °C and 39.9 psu in winter, and equal to 20.7 °C and 39.0 psu in summer (Bower *et al.* 2000). RSW spreads and diffuses across the Gulf of Aden between 400 and 800 meters depth (Bower *et al.* 2005). In the Gulf of Aden, the surface flow is dominated by mesoscale eddies (Al Saafani *et al.* 2007). These eddies are long lived, and deeply reaching (Morvan *et al.* 2020), and they have an impact on the fate of RSW (Bower and Furey 2012). *In situ* observations have shown a three-layer (two-layer) in summer (winter) exchange at the Strait of Bab El Mandeb (Murray and Johns 1997, Smeed 2004), but in this paper we consider only a two-layer exchange so that the RSW outflow is a bottom buoyant current. We propose to study the dynamics of a bottom buoyant current flowing in a semi-enclosed basin with a primitive equation model, in an idealized approach.
Nof *et al.* (2002) studied the influence of the slope of the bathymetry on the formation of

lenses of RSW, namely Reddies. Bower *et al.* (2002) have shown that the RSW outflow can be considered as a western boundary undercurrent and the generation of a cyclonic circulation due to vortex stretching as the RSW outflow cascades down to its neutral buoyancy level. Aiki *et al.* (2006) showed that the discharged RSW is always characterized by anticyclonic vorticity. With a primitive equation model, Ilıcak *et al.* (2011) concluded that mesoscale eddies alter the transport and the mixing of RSW. Furthermore, the Gulf of Aden is composed of bathymetric features which potentially impact the RSW outflow. We clearly identify two of them. First, downstream of the Strait of Bab El Mandeb, a zonal rift is localized at the western end of the Gulf of Aden, namely the rift of Tadjurah. Second, the northern and the southern coasts of the Gulf of Aden are curved with capes.
We adress the following questions: Do the bathymetric features, such as rift and cape, have an impact on the bottom buoyant current? How the bottom buoyant current vertically equilibrates? How the bottom buoyant current horizontally diffuses across the basin? Do the bottom buoyant current dynamics depend on the season? We compare idealized primitive equations simulations in which we progressively add topographic and dynamical elements. The model configuration and initialization are presented in section 2. The results are shown in section 3 and discussed in section4. The conclusion is drawn in section 5.

2. Model configuration and initialization

2.1. *Model configuration*

We use the Coastal and Regional Ocean COmmunity (CROCO, Shchepetkin and McWilliams (2005)) model, which is a free surface, primitive equation model based on the hydrostatic assumption that uses "terrain-following" vertical coordinates. The momentum and tracers equations are solved using the 5^{th} order upstream-biased advection scheme on the horizontal, and the splines vertical advection scheme on the vertical. The horizontal grid resolution is 1 km. The time step is $\delta t = 270\,\text{s}$ so that the CFL-criterion is satisfied. The integration period is 200 days, and the outputs are saved every 6 hours. The semi-enclosed basin is 800 km long, 200 km wide and 2000 m deep. The Coriolis frequency is defined as

$$f \;=\; f_0 + \beta y\,, \tag{1}$$

where $f_0 = 6 \times 10^{-5}\,\text{s}^{-1}$ is the mean Coriolis frequency in the Gulf of Aden and $\beta = 2 \times 10^{-11}\,\text{m}^{-1}\text{s}^{-1}$ is the mean gradient of the planetary vorticity. 50 vertical levels are used with finer vertical resolutions at the surface and the bottom bathymetry (the surface and bottom stretching parameters are, respectively, $\theta_\text{s} = 3$ and $\theta_\text{b} = 3$). At shallow depth, the vertical spacing goes from 1 to 10 meters. In the deep ocean, the vertical spacing varies between 10 to 60 meters. The surface and bottom vertical mixing is parameterized with a KPP-scheme (Large *et al.* 1994). We do not implement any atmospheric forcing at the surface. At the bottom, we use the Von-Kármán quadratic bottom stress formulation defined as

$$\tau_\text{b} \;=\; \rho_0 C_D ||\boldsymbol{u}||\,\boldsymbol{u}\,, \tag{2}$$

where ρ_0 is a reference density. C_D is the drag coefficient varying as

$$C_D \;=\; \left(\frac{\kappa_\text{vk}}{\log\left(\Delta z_b / z_r\right)}\right)^2\,, \tag{3}$$

where κ_vk is the Von-Karman constant equal to 0.41 (von Karman 1912), z_r is the roughness parameter equal to 1 cm and Δz_b is the thickness of the lowest layer of the grid. Western and southern boundaries are closed, while northern and eastern boundaries are opened (see figure 1).

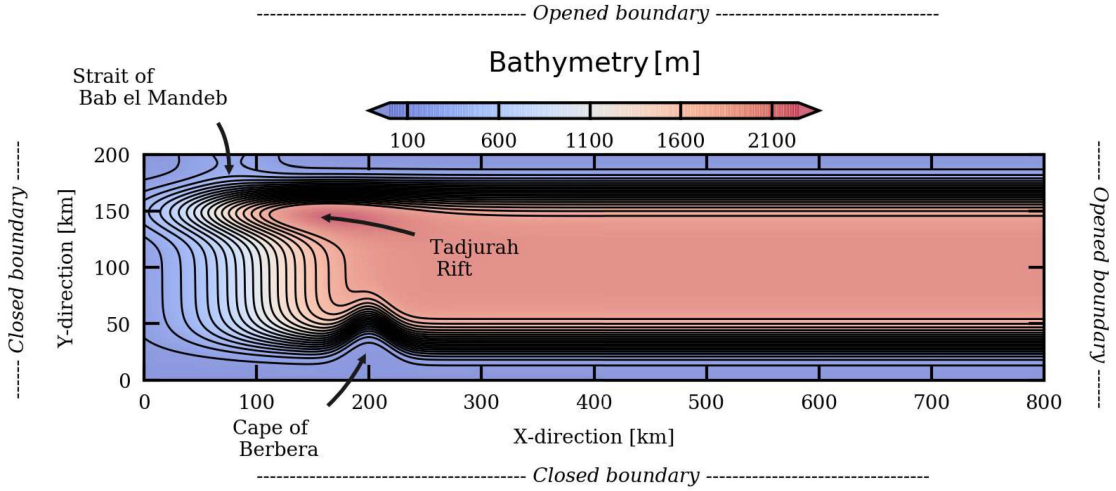

Figure 1. Bathymetry of the domain of integration. (Colour online)

2.2. *Idealized bathymetry*

The bathymetry is designed to ressemble that of the Gulf of Aden. It consists of continental slopes north, west and south of the domain, an idealized Strait of Bab El Mandeb, an idealized Tadjurah Rift, and an idealized cape of Berbera south of the domain (figure 1). The bathymetry is implemented as follows

$$h = H\left[1-\exp\left(-\frac{(x+x_0)^4}{w_x^4}\right)\right]\exp\left(-\frac{(y^*-y_0)^6}{w_y^6}\right)+h^{\mathrm{BEM}}+h^{\mathrm{TAJ}}, \tag{4}$$

where

$$h^{\mathrm{BEM}} = H^{\mathrm{BEM}}\exp\left[-\left(\frac{x-x^{\mathrm{BEM}}}{w_x^{\mathrm{BEM}}}\right)^2-\left(\frac{y-y^{\mathrm{BEM}}}{w_y^{\mathrm{BEM}}}\right)^2\right], \tag{5}$$

$$h^{\mathrm{TAJ}} = H^{\mathrm{TAJ}}\exp\left[-\left(\frac{x-x^{\mathrm{TAJ}}}{w_x^{\mathrm{TAJ}}}\right)^2-\left(\frac{y-y^{\mathrm{TAJ}}}{w_y^{\mathrm{TAJ}}}\right)^2\right], \tag{6}$$

and

$$y^* = \begin{cases} y\,, & \text{if } y < 100\mathrm{km} \\ y + y_0^{\mathrm{CAP}}\exp\left[-\left(\dfrac{x-x^{\mathrm{CAP}}}{w^{\mathrm{CAP}}}\right)^2\right], & \text{if } y > 100\mathrm{km} \end{cases} \tag{7}$$

with $H = 2000\,\mathrm{m}$, $x_0 = y_0 = 100\,\mathrm{km}$, $w_x = 220\,\mathrm{km}$, $w_y = 70\,\mathrm{km}$, $x_0 = 100\,\mathrm{km}$, $H^{\mathrm{BEM}} = 250\,\mathrm{m}$, $x^{\mathrm{BEM}} = 75\,\mathrm{km}$, $y^{\mathrm{BEM}} = 200\,\mathrm{km}$, $w_x^{\mathrm{BEM}} = 40\,\mathrm{km}$, $w_y^{\mathrm{BEM}} = 80\,\mathrm{km}$, $H^{\mathrm{TAJ}} = 800\,\mathrm{m}$, $x^{\mathrm{TAJ}} = 110\,\mathrm{km}$, $y^{\mathrm{TAJ}} = 150\,\mathrm{km}$, $w_x^{\mathrm{TAJ}} = 100\,\mathrm{km}$, $w_y^{\mathrm{TAJ}} = 20\,\mathrm{km}$, $y_0^{\mathrm{CAP}} = 20\,\mathrm{km}$, $x^{\mathrm{CAP}} = 200\,\mathrm{km}$, and $w^{\mathrm{CAP}} = 25\,\mathrm{km}$. Note that h^{TAJ} modeling the Rift of Tadjurah, and y_0^{CAP} modeling the Cape of Berbera, can be set to 0 if no Rift of Tadjurah and/or no Cape of Berbera are considered.

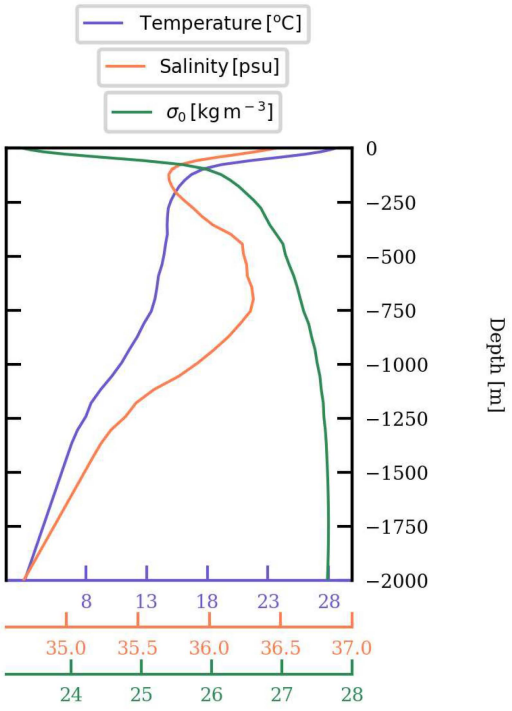

Figure 2. Background (blue) temperature, (red) salinity and (green) potential density. (Colour online)

2.3. *Background stratification*

The background stratification comes from the climatological temperature and salinity profiles provided by Argo floats in the Gulf of Aden (see figure 2). We linearly interpolate the Argo data on the 50 vertical levels of the model. The background stratification is initially horizontally uniform in the whole domain of integration.

2.4. *Idealized bottom buoyant current*

The idealized flow is a bottom buoyant current (BBC) implemented as a forcing over the whole water column uniform in time in the northern open-boundary (at $y = 200\,\mathrm{km}$)by setting a temperature and salinity anomalies defined as

$$T' = \tfrac{1}{2}(\Delta T)F_1(x)F_2(z)\,, \tag{8}$$

and

$$S' = \tfrac{1}{2}(\Delta S)F_1(x)F_2(z)\,, \tag{9}$$

where

$$F_1(x) = 1 - \tanh\left(\frac{x - x^{ts}}{w_x^{ts}}\right), \qquad F_2(x) = \exp\left[-\left(\frac{z - z^{ts}}{w_z^{ts}}\right)^2\right]$$

with $x^{ts} = 75\,\mathrm{km}$, $w_x^{ts} = 10\,\mathrm{km}$, and $z^{ts} = -200\,\mathrm{m}$. ΔT, ΔS, and w_z^{ts} depend on the seasons (see Table 1). These values are based on the winter and summer properties of the RSW as listed in Bower *et al.* (2000) in their Table 2. Then, the velocity components of the overflow is

	Winter	Summer
ΔT [°C]	6	4
ΔS [psu]	4	3
w_z^{ts} [m]	100	50

Table 1. Bottom buoyant current properties.

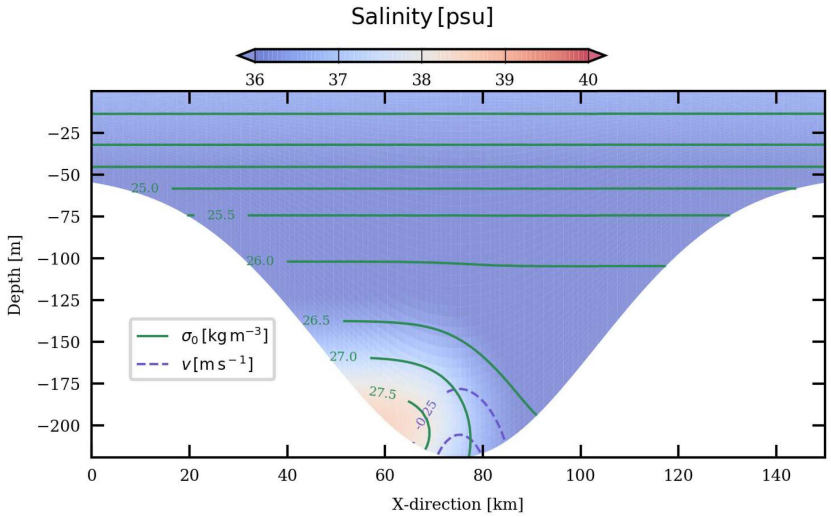

Figure 3. Bottom buoyant current structure in winter, implemented in the northern open boundary. The salinity is represented in color. The density and the meridional velocity component are respectively drawn in green and blue contours. (Colour online)

computed *via* the thermal wind balance (see figure 3). The Sea Surface Height (SSH) is directly computed from the density anomaly by a vertical integration of the hydrostatic balance.

2.5. *Mesoscale eddies*

The mesoscale eddies are initialized following the procedure in Ciani *et al.* (2016) and Morvan *et al.* (2019). The velocity field of each eddy is defined as

$$v_\theta(r,z) = \pm\frac{v_0 r}{R}\exp\left(-\frac{r^2}{R^2}\right)\exp\left(-\frac{z^2}{D^2}\right), \tag{10}$$

with $v_0 = 0.5\,\mathrm{m\,s^{-1}}$, $R = 50\,\mathrm{km}$, $D = 1000\,\mathrm{m}$, typical values found in the Gulf of Aden (Bower and Furey 2012). Then, the pressure field is computed *via* the cyclo-geostrophic balance as described in Ciani *et al.* (2016). The density anomalies associated with the mesoscale eddies are computed using the hydrostatic equilibrium. Mesoscale eddies are separated by 150 km from each other and by 100 km from the southern and northern coasts (see figure 4).

To investigate the dynamics of such a BBC, a set of simulations is performed in which we modify the shape of the bathymetry, the properties of the overflow depending on the season, and we add mesoscale eddies. The simulations are named and summarized in the Table 2.

2.6. *Lagrangian tracking*

We use the ARIANE tool (Blanke and Raynaud 1997) to investigate (1) the impact of mesoscale and submesoscale eddies on the spreading of the overflow water from the Strait

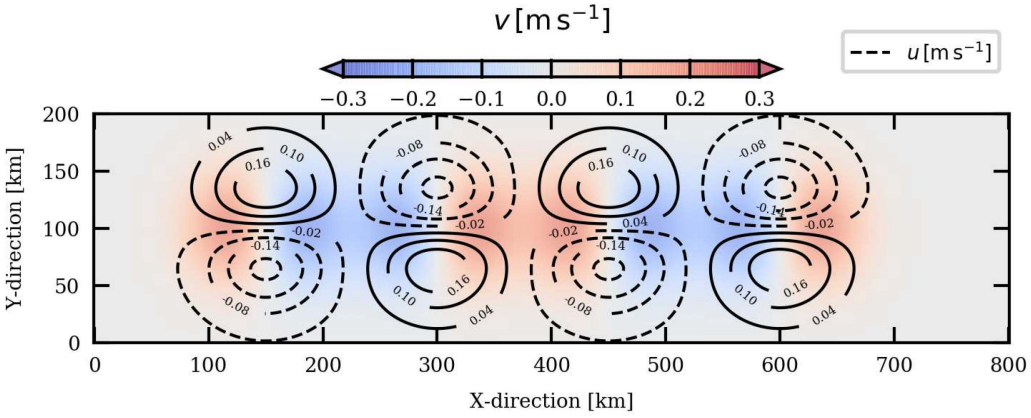

Figure 4. Surface velocity structure of the mesoscale eddies initially implemented. The colors and the contours stand for the meriodional and the zonal velocity components respectively. (Colour online)

	Winter	Summer	Tadjurah Rift	Cape of Berbera	Mesoscale eddies
W-ref	✓	-	-	-	-
W-taj	✓	-	✓	-	-
W-glo	✓	-	✓	✓	-
S-glo	-	✓	✓	✓	-
W-ed1	✓	-	✓	✓	C-A-C-A
W-ed2	✓	-	✓	✓	A-C-A-C

Table 2. Set of numerical experiments. A and C means respectively anticyclone and cyclone.

of Bab el Mandeb towards the eastern boundary, and (2) the isopycnal *vs* the diapycnal mixings of the RSW. ARIANE is a computational tool dedicated to the offline calculation of 3D streamlines in the output velocity field of model whose equations are based on volume-conserving numerical formulation. Transports of water masses or currents are deduced from the displacement of numerical Lagrangian particles.

3. Results

3.1. *BBC vertical adjustment*

The spatial and time evolutions of the RSW distribution depend on the evolution of the BBC, linked to the topographic elements as shown in figure 5. As the BBC exits the Strait of Bab El Mandeb, the salinity loses about 2 psu and the associated density goes from 27.8 to 27.2 kg m^{-3}. Diapycnal mixing occurs during the BBC diving from 200 down to 450 m depth. Note that the diapycnal mixing is strengthened by the Tadjurah Rift. Then, the BBC reaches the position of the Cape of Berbera. There, submesoscale eddies are generated. The RSW loses about 0.25 psu due to isopycnal mixing since the RSW does not experience any substantial density variation.

An instantaneous view of the salinity maxima as well as the corresponding density and depth, is shown in figure 5. In all experiments, the BBC enters the semi-enclosed basin through the idealized Strait of Bab El Mandeb which is about 200 meters deep. The BBC flows over the continental shelf and cascades down to the depth of its neutral density after vertical mixing has occured. As pointed out by L'Hégaret *et al.* (2020), the RSW outflow stabilizes on the

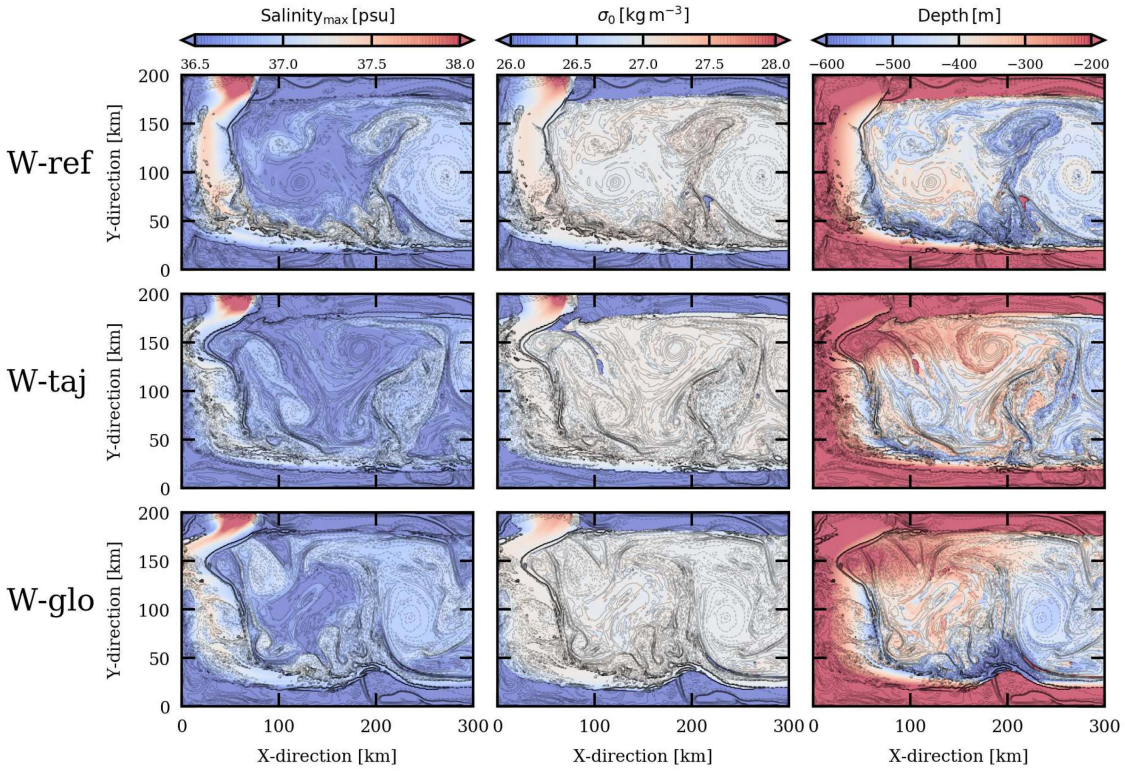

Figure 5. Snapshots at day 150 of (left) the salinity maximum over the water column, and (middle and right) the corresponding density and depth. Contours stand for the vertical relative vorticity. (Colour online)

27.0 kg m^{-3} isopycnal level on average. Once stabilized, the BBC locates between 300 and 600 m depth. Farther from the strait, the outflow progressively expands vertically.

The vertical adjustment of the BBC and the effect of the Tadjurah Rift is highlighted by Lagrangian experiments performed with the W-ref and W-taj experiments. About 20000 particles are initially seeded in the Strait of Bab El Mandeb at grid points where salinity is larger than 39 psu. The time evolutions of the ensemble average of positions, thermohaline properties are shown in figure 6. From the particle's trajectories, we estimate the vertical diffusivity of salinity (K_z in figure 6) by considering the diffusion equation

$$\mathrm{d}_t S \;=\; K_z\, \partial^2_{zz} S\,, \tag{11}$$

where $\mathrm{d}_t S$ is directly computed from the particles trajectories, and $\partial^2_{zz} S$ is computed from the model outputs. Then, the vertical diffusivity of salinity is estimated as

$$K_z \;=\; \frac{\langle\, \mathrm{d}_t S \,\rangle}{\langle\, \partial^2_{zz} S \,\rangle}\,, \tag{12}$$

where $\langle \bullet \rangle$ stands for an ensemble average. The Lagrangian experiments show that the BBC experiences vertical mixing. In the W-ref experiment, the salinity and temperature decrease respectively from 39 to 37 psu, and from 20.5 to 17°C in about 3 days. This corresponds to the vertical density adjustment of the overflow in the gulf. Indeed, in the Strait of Bab El Mandeb, the particles are located at 200 m depth. As particles exit the strait, they are denser than the surrounding fluid parcels. Thus they dive down to about 400 m depth. During the diving, vertical mixing occurs resulting in the equilibration of the BBC on the 27.0 kg m^{-3} density level. The corresponding maximum vertical diffusivity coefficient is estimated to about

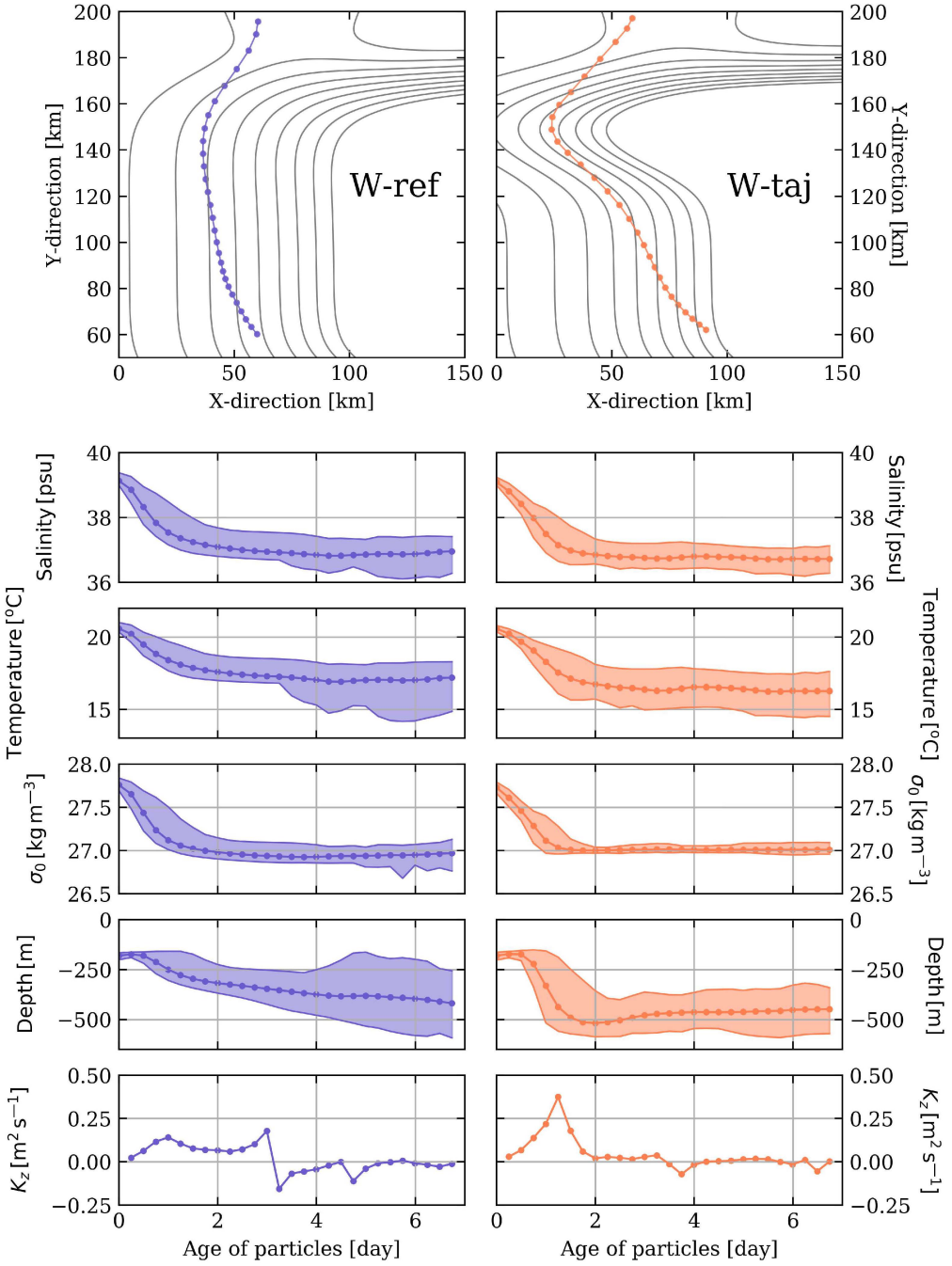

Figure 6. Results from Lagrangian experiments. From top to bottom: Time evolution of the ensemble average of the position (solid grey lines stand for the contours of bathymetry), salinity, temperature, density, depth and vertical diffusivity of particles in the (blue) W-ref and (orange) W-taj experiments. (Colour online)

$0.2\,\mathrm{m^2\,s^{-1}}$. The BBC reaches its neutral density in 3 days, while it monotonically dives in a week, down to about 400 m depth.

In the presence of the Tadjurah Rift, both the neutral density and the equilibrium depth are reached in 3 days due to stronger vertical mixing. The curvature of the mean trajectory of particles indicates that the centrifugal acceleration of the flow generates ageostrophic motions associated with vertical motions (see figure 7). The maximum vertical diffusivity of salinity K_z corresponds to the maximum of vertical velocity and is located on the bottom slope.

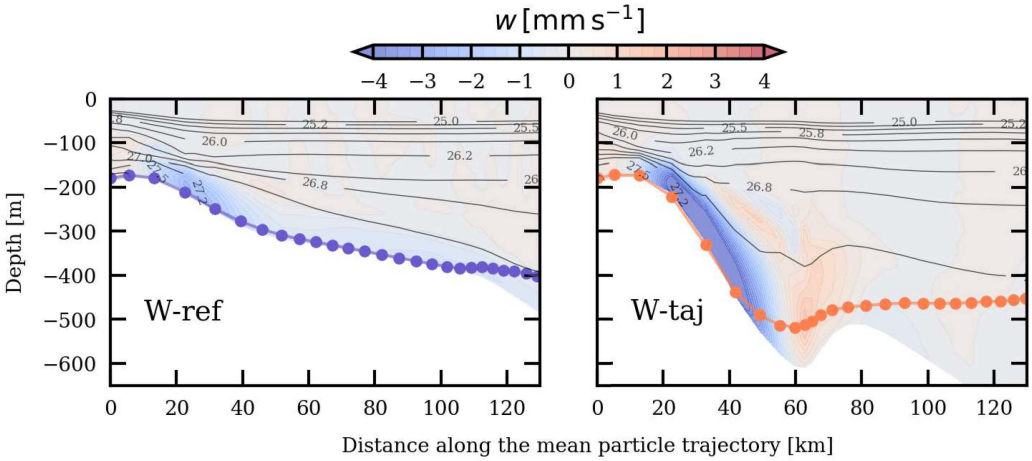

Figure 7. Vertical slice of vertical velocity along the mean trajectory of particles (shown in figure 6). Density contours are shown in solid black lines. The mean positions of particles are drawn in blue and orange for the W-ref and the W-taj experiments respectively. (Colour online)

3.2. *BBC water diffusion through isopycnal mixing*

Once the BBC equilibrates at depth, the BBC water is mixed with surrounding water through isopycnal mixing as it spreads in the semi-enclosed basin. The time series of the particles ensemble average of salinity, temperature, density, depth and horizontal diffusivity of salinity are shown in figure 8. The horizontal diffusivity of salinity is computed considering the following diffusion equation

$$\mathrm{d}_t S = K_h \nabla^2 S \,. \tag{13}$$

Then, the horizontal diffusivity of salinity is estimated as

$$K_h = \frac{\langle \mathrm{d}_t S \rangle}{\langle \nabla^2 S \rangle} \,, \tag{14}$$

where $\langle \bullet \rangle$ stands for an ensemble average.

The thermohaline properties of particles vary little compared to diapycnal mixing arising upstream. In the absence of the Cape of Berbera (W-taj experiment), the horizontal diffusivity of salt increases for the particles about 10 days after their release. This is the signature of the BBC water mixing with the surrounding water. However the horizontal diffusivity of salinity is significantly weaker in the presence of the Cape of Berbera (W-glo experiment).

To highlight the role of the Cape of Berbera on the weakening of the horizontal diffusivity of the BBC water, we compare the normalized probability density function (PDF) of the salinity and the vertical relative vorticity normalized by the Coriolis frequency shown in figure 9. The salinity of particles is comprised between 36 and 37 psu in both the W-taj and W-glo experiments. The shapes of the PDF are in agreement with the previous result stating that the horizontal mixing is more important in the W-taj experiment without the Cape of Berbera. The normalized PDF of the vertical relative vorticity associated with particles is centered around 0. This means that most particles are in a irrotational zone. Intense relative vorticity (i.e. $|\zeta^z/f_0| \geq 0.5$) is reached meaning that particles are also trapped into anticylonic and cyclonic eddies. Note that the PDF is asymmetric. A larger number of particles is trapped in anticyclones when the Cape of Berbera is not included compared to when it is which induces a better salt conservation. This suggests that the Cape of Berbera has an impact on the production of negative vorticity along the southern coast. Thus, the horizontal diffusion

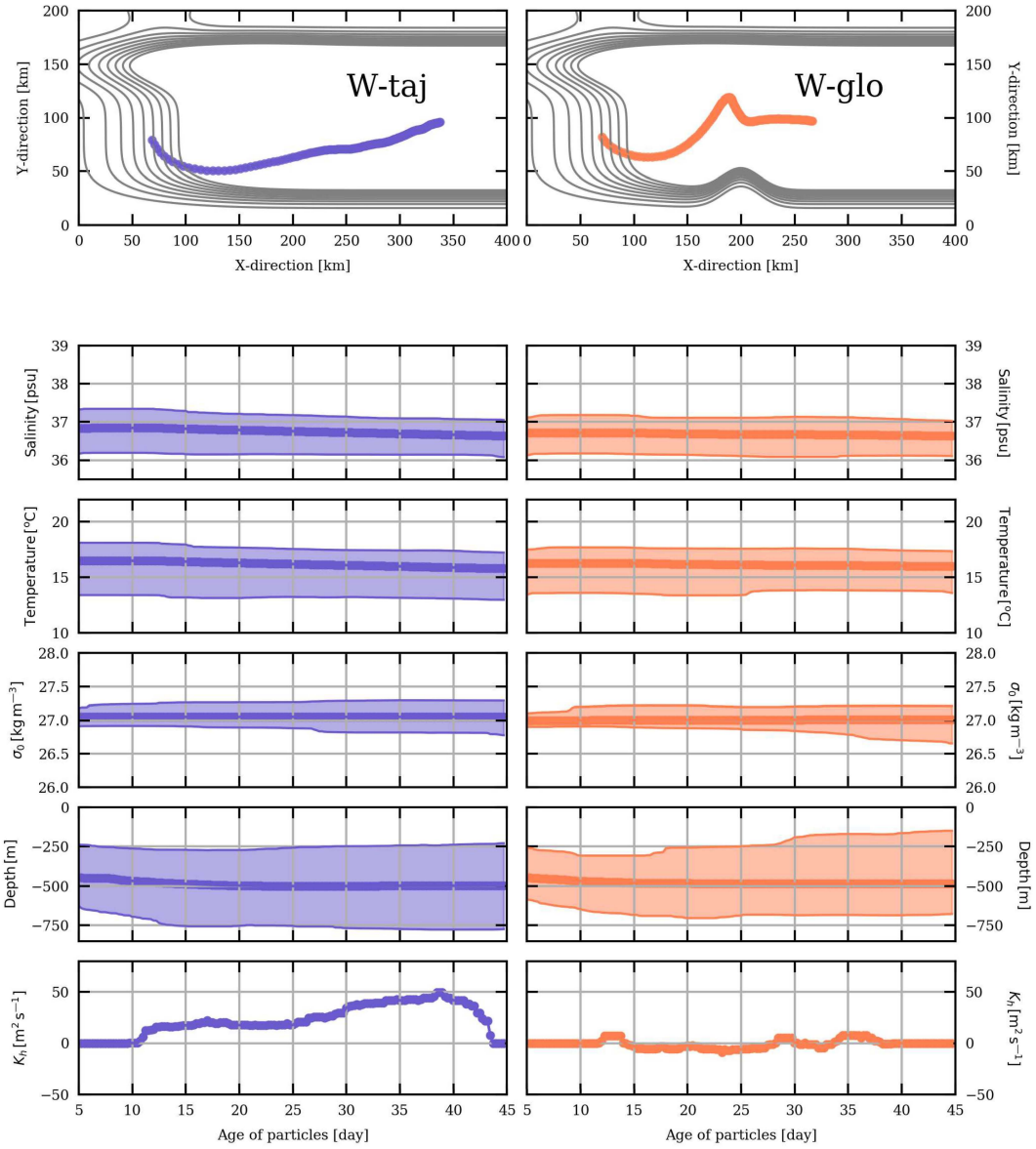

Figure 8. Results from Lagrangian experiments. From top to bottom: Time evolution of the ensemble average of the position, salinity, temperature, density, depth and horizontal diffusivity of particles in the (blue) W-taj and (orange) W-glo experiments. (Colour online)

of salinity depends on the dynamics at the Cape of Berbera. The dynamics at the Cape of Berbera is studied in the following section.

3.3. *An unstable BBC and the generation of eddies*

In the absence of atmospheric forcing as well as surrounding mean flow, the BBC experiences instabilities. Eddies form during the first 50 days A quasi-stationary mesoscale dipole cyclone/anticyclone is located at the Cape of Berbera. The cyclone (West) and the anticyclone (East) have a radius of about 50 km and a maximum azimuthal velocity of about $0.5\,\mathrm{m\,s^{-1}}$. The dipole cyclone/anticyclone is sub-surface intensified and participates in the spreading of the RSW. We study its generation mechanism in the following section. Submesoscale eddies

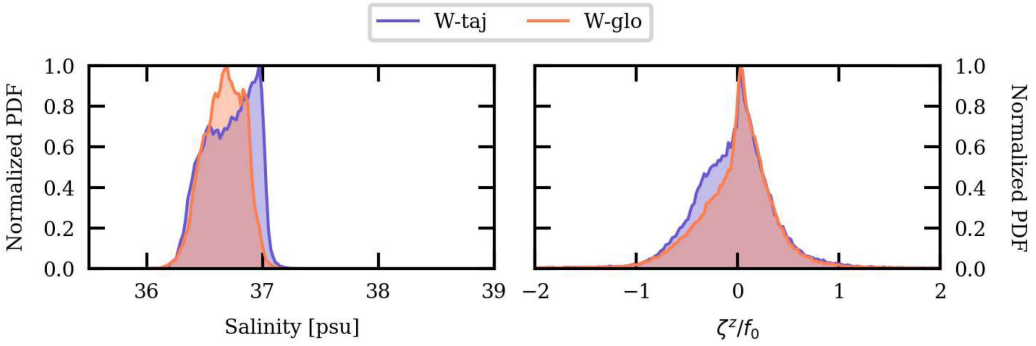

Figure 9. Normalized Probability Density Function of (left) salinity, and (right) vertical relative vorticity normalized by the Coriolis frequency of particles in (blue) the W-taj, and (orange) the W-glo experiments. (Colour online)

are also formed in the vicinity of the rift, and along the continental slopes. In this section, we study the generation of eddies in terms of potential vorticity anomaly (PVa) and energy conversions. The PVa is defined by

$$Q' = Q - Q_0 \,. \tag{15}$$

Q is the Ertel's potential vorticity

$$Q = \boldsymbol{\zeta_a} \cdot \boldsymbol{\nabla} b \,, \tag{16}$$

where $\boldsymbol{\zeta_a}$ is the absolute vorticity and b is the buoyancy. Q_0 is the background potential vorticity (i.e. the potential vorticity at rest)

$$Q_0 = f \partial_z \overline{b} \,, \tag{17}$$

where $\overline{b}$ is the stratification at rest.

The energy sources are the Horizontal Reynolds Stress (HRS), the Vertical Reynolds Stress (VRS), and the Vertical Buoyancy flux (VBF) (Gula *et al.* 2016). The HRS and VRS are related to the transfer of mean kinetic to eddy kinetic energy through horizontal (or barotropic) and vertical (Kelvin-Helmholtz type) shear instabilities respectively. The VBF reflects the conversion of mean potential to eddy kinetic energy through baroclinic instability. They are

$$\text{HRS} = -\overline{\boldsymbol{u}'v'} \cdot \partial_y \overline{\boldsymbol{u}} - \overline{\boldsymbol{u}'u'} \cdot \partial_x \overline{\boldsymbol{u}} \,, \tag{18}$$

$$\text{VRS} = -\overline{\boldsymbol{u}'w'} \cdot \partial_z \overline{\boldsymbol{u}} \,, \tag{19}$$

$$\text{VBF} = \overline{w'b'} \,, \tag{20}$$

where u,v and w are the zonal, the meridional and the vertical velocity components, $\overline{\bullet}$ denote the time average, and $\bullet'$ the deviation from the time average.

3.3.1. *The dipole cyclone/anticyclone structure*

A mesoscale dipole cyclone/anticyclone forms in all our simulations. We present the mesoscale dipole cyclone/anticyclone in the W-ref experiment in figure 10, where the bathymetry consists of continental slopes without uneven bathymetry. The dipole cyclone/anticyclone is composed of a sub-surface intensified western cyclone and of a sub-surface intensified eastern anticyclone. Both eddies are about 50 km in radius, and 1000 m thick. The maximum potential vorticity of the cyclone and the anticyclone can reach about $150\% \times Q_0$ (in absolute value).

The anticyclone exhibits a larger (in absolute value) negative PVa in its core than in the

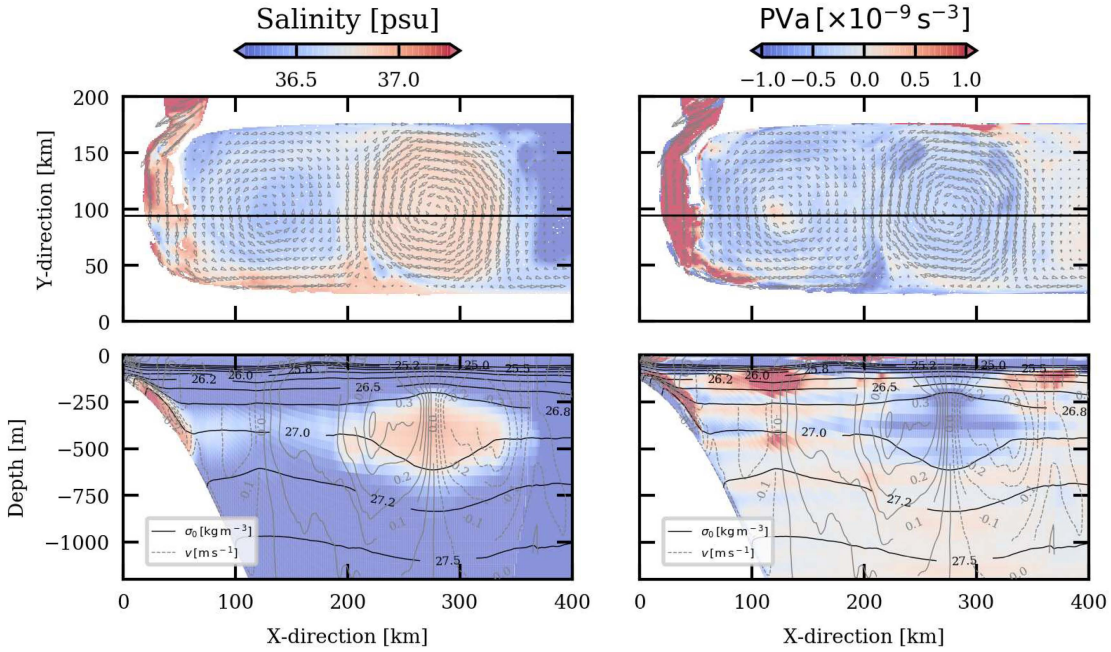

Figure 10. Results from the W-ref experiment averaged from day 145 to day155. Top row: Horizontal slices of (left) salinity and (right) PVa interpolated on the $27.0\,\mathrm{kg\,m^{-3}}$ isopycnic level. The arrows stand for the velocity vectors interpolated on the same isopycnic level. Bottom row: Vertical sections (black solid line indicated in the top panels) of (left) salinity and (right) PVa. isopycnic levels and meridional velocity component are indicated in black and grey solid lines respectively. (Colour online)

core of the cyclone. The anticyclone core is centered at 350 m depth. The negative PVa of the anticyclone is associated with a positive salinity anomaly which is the signature of the salty water of the BBC. The thermohaline structure of the anticyclone is confined roughly between the 26.5 and $27\,\mathrm{kg\,m^{-3}}$ isopycnic levels (below the thermocline), while the dynamical structure can extend from the surface down to about 1000 meter depth.
The structure of the cyclone is more complex. On the $27\,\mathrm{kg\,m^{-3}}$ isopycnic level, the core of the cyclone is slightly positive in term of potential vorticity anomaly. This is in agreement with the absence of positive density anomaly, so that in the core of the cyclone, the potential vorticity is not far from the background one ($Q \sim Q_0$). At the periphery, the potential vorticity anomaly is negative due to the submesoscale fragments of RSW advected around the cyclone on the $27\,\mathrm{kg\,m^{-3}}$ isopycnic level. The vertical section of PVa shows that the cyclone is composed of an alternance of positive and negative PVa on the vertical. This is a clue of the primary source for the dipolar eddy generation. This suggests that the dipole cyclone/anticyclone forms due to baroclinic processes. Also, the PVa of the BBC changes sign on the vertical as it flows over the sloping bathymetry (see figure 10, vertical section of PVa between 0 and 50 km from the coast). This is a necessary condition for baroclinic instability to occur (Charney and Stern 1962).

3.3.2. *A baroclinic instability as the origin of the dipole cyclone/anticyclone generation*

The main source terms in the vorticity equation are the bottom pressure torque and the bottom drag curl (Gula *et al.* 2015). Along the southern coast of the basin, the intensity of the bottom pressure torque and the bottom drag curl substantially decreases (see figure 11 (a)). Their minimum values are reached for $x \in [150; 250]$ km. At this location the mean flow interaction with the sloping bathymetry is weak. Indeed, it corresponds to the location of

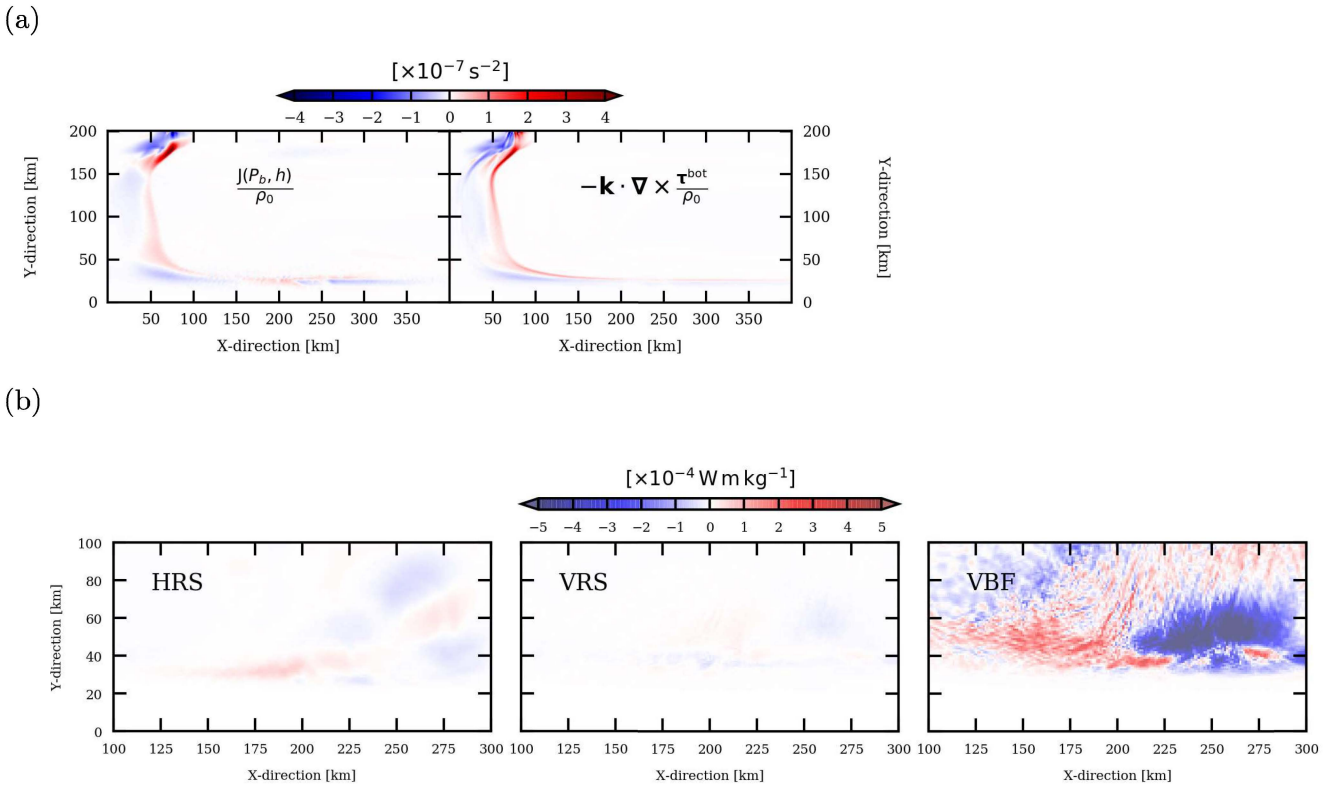

Figure 11. Results from the W-ref experiment averaged from day 75 to day 100 corresponding roughly to the period of formation of the dipole cyclone/anticyclone. (a) Bottom pressure torque (left) and bottom drag curl (right). (b) Energy conversion terms vertically integrated between 300 and 600 m depth: HRS (left), VRS (middle) and VBF (right). (Colour online)

the formation of the dipole cyclone/anticyclone. To highlight the primary instability generating the dipolar eddy, we compute the energy conversion term averaged over the period of its formation, and integrated between 300 and 600 m depth (see figure 11 (b)). The vertical buoyancy flux prevails on the horizontal and the vertical shear production. The vertical buoyancy flux has a positive signal where the baroclinic instability is triggered. This means that the mean potential energy of the BBC is converted into eddy kinetic energy. The BBC undergoes baroclinic instability as it flows over the southern sloping bathymetry resulting in the formation of a mesoscale dipole cyclone/anticyclone.

3.3.3. *Life cycle of the dipole cyclone/anticyclone and submesoscale eddies generation*

As mentioned previously, the dipole cyclone/anticyclone forms in all experiments *via* baroclinic instability. Nonetheless, the subsequent evolution of the dipole cyclone/anticyclone varies between experiments. The life cycle of the dipole cyclone/anticyclone strongly depends on the bathymetric features. Time sequences of the vertical relative vorticity normalized by the Coriolis frequency at 400 m depth are shown in figure 12.

In the experiment without any Tadjurah Rift (W-ref), the dipole cyclone/anticyclone is quasi-stationary, and submesoscale eddies are generated by viscous interactions. These submesoscale eddies can be cyclonic or anticyclonic. They are advected at the periphery of the mesoscale eddies. Submesoscale anticyclones merge with the mesoscale anticyclone. In the experiments with the Tadjurah Rift (W-taj and W-glo), the dipole cyclone/anticyclone moves northward. At the northern coast of the domain, the dipole cyclone/anticyclone should have separated as explained by the image-vortex theory with the cyclone propagating westward

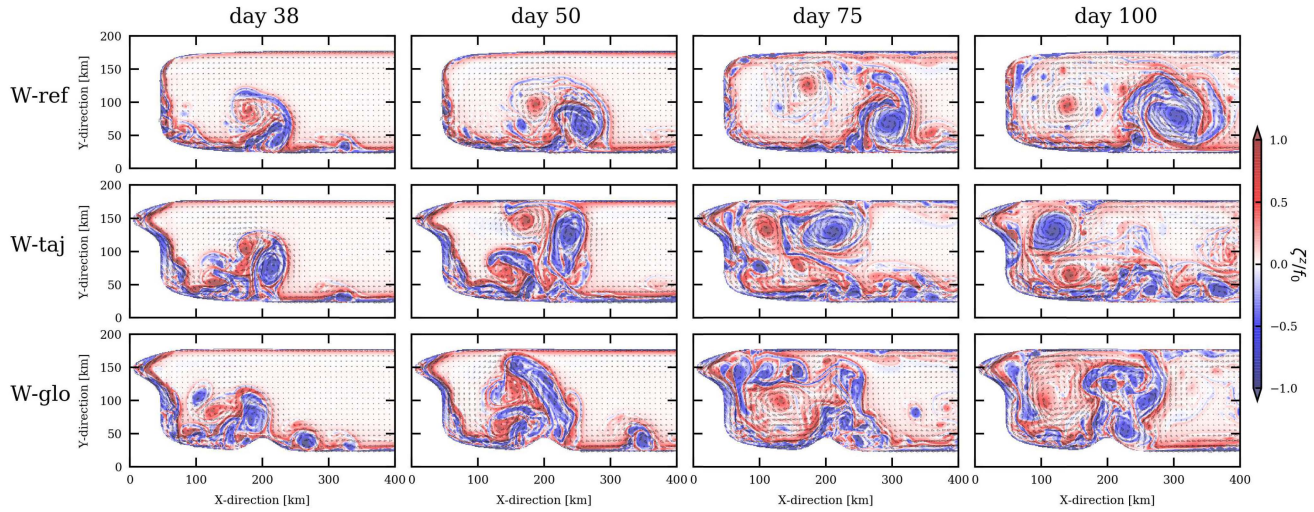

Figure 12. Time sequences of the relative of vertical relative vorticity normalized by the Coriolis frequency. (Colour online)

and the anticyclone propagating eastward (Shi and Nof 1994). On the contrary, both eddies propagate westward. This is the signature of the Tadjurah Rift effect. The bathymetry steers the vortex drift. Simultaneously, submesoscale eddies are produced along the southern coast of the domain.

The mechanism generating submesoscale eddies is associated with the bottom drag of mesoscale eddies over the sloping bathymetry (Morvan *et al.* 2019). A subsequent bottom boundary layer vorticity filament is generated which can detach from the continental slope, and forms submesoscale eddies through horizontal shear instability. This is confirmed by the computation of the energy transfer terms (see figure 13). In all experiments, the horizontal shear production prevails on the other terms (i.e. HRS $\gg$ VBF $\gg$ VRS). So, as the BBC drags over the continental slope, the bottom frictional layer experiences horizontal shear instabilities leading to the production of submesoscale eddies. Note that the buoyancy flux is slightly positive meaning that the BBC is still baroclinically unstable.

In the absence of Tadjurah Rift (in the W-ref experiment), the quasi-stationary mesoscale cyclone (part of the dipole cyclone/anticyclone) in conjunction with the BBC induce the generation of an intense horizontal shear production leading to the formation of intense anticyclonic eddies ($\zeta^z/f < -1$). Some of them are advected at the periphery of the mesoscale cyclone forming a constellation of satellites around it (see figure 12, W-ref experiment at day 100). The other satellites interact with the mesoscale anticyclone and subsequently merge with it (see figure 12, W-ref experiment at day 75). These submesoscale anticyclones participate to the sustainment of the mesoscale anticyclone.

In the presence of the Tadjurah Rift, the dipole cyclone/anticyclone starts to propagate northward due to its self-advection, then it propagates westward (see figure 12, 3$^{\text{rd}}$ row). As it propagates northward and flows over the rift, the depth of the water column increases. In order for the dipole's potential vorticity to be conserved, positive relative vorticity has to be created resulting in the westward propagation of the dipole cyclone/anticyclone. The westward propagation of the dipole cyclone/anticyclone allows the BBC to flow over the continental slope. Still, the BBC is baroclinically unstable, and dipolar eddies are subsequently generated. Note that submesoscale eddies are also generated due to the bottom boundary layer detachment. These submesoscale eddies propagate mostly zonally and eastward over the continental slope in the W-taj experiment (without cape). In the presence of the Cape of Berbera (see figure 12, W-glo experiment), the submesoscale anticyclonic eddies merge

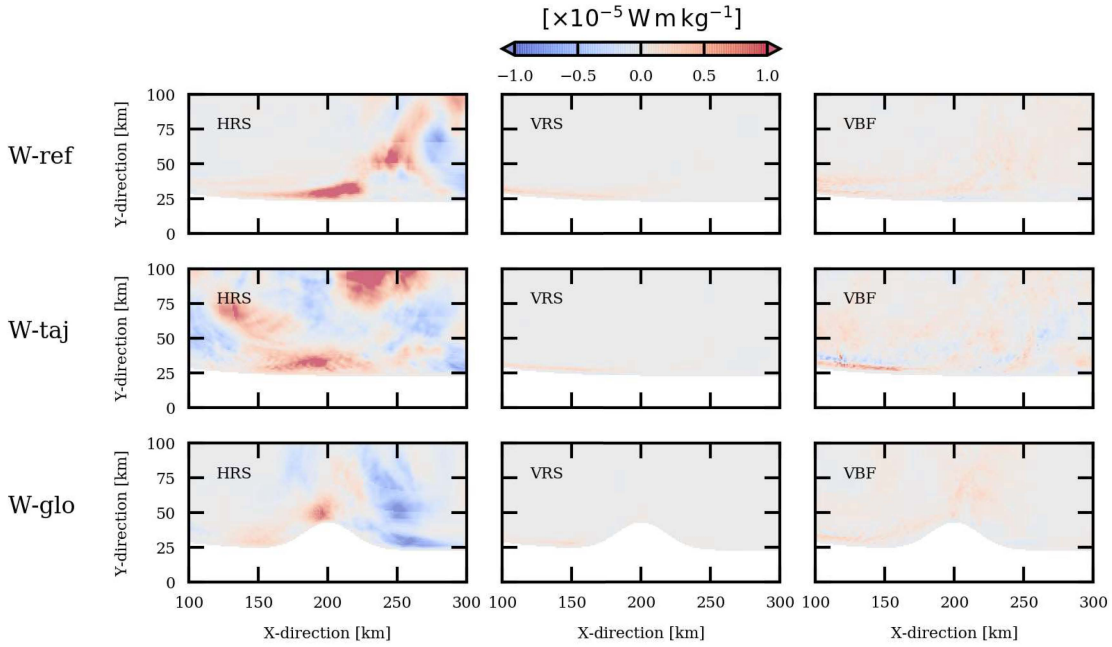

Figure 13. Results from the W-ref, W-taj and W-glo experiments. Energy conversion terms averaged between day 50 and 150 of integration time, and vertically integrated between 350 and 450 m depth. (Colour online)

together, and finally form an anticyclonic mesoscale motion similar to the one arising in the W-ref experiment.

The Power Spectrum Density (PSD) of the horizontal velocities and the vorticity are shown in figure 14. At submesoscale (i.e., the spatial scale below the deformation radius equal to 50 km), the slopes of the spectra are identical for all experiments. The slope of the spectra depends at the depth level they are computed. Indeed, in all experiments the bathymetry is not flat. The bathymetry is composed of the Strait of Bab El Mandeb, and the northern, southern and western continental slopes. The Cape of Berbera and the Rift of Tadjurah are implemented afterward. The -6 and -3 (at $z = -50\,\mathrm{m}$), and the -4 (at $z = -400\,\mathrm{m}$) spectral slopes suggest an energetic submesoscale dynamic develop in the presence of bathymetry, in particular the continental slopes. At $z = -1000\,\mathrm{m}$, the -2 spectral slope indicates a gentler transition between the mesoscale and the submesoscale dynamics where the continentale slopes are gentler as well. The submesoscale fields are the most energetic at sub-surface ($z = -400\,\mathrm{m}$). The enstrophy spectra indicate that these submesoscale flows are eddies or filaments with strong vorticity. We also observe that submesoscale eddies are the most active in the experiments for which the Tadjurah Rift is implemented (i.e., W-taj and W-glo). The impact of the Cape of Berbera is also highlighted since the W-ref experiment is the less energetic experiment. Finally, in the presence of a mesoscale eddy field initially (W-ed1), a sub-surface submesoscale eddy field still arises but less energetically than the one evolving in the other experiments. Near the surface ($z = -50\,\mathrm{m}$), the flow is more quiescent. Submesoscale eddies can exist but they are less energetic than at sub-surface. At depth ($z = -1000\,\mathrm{m}$), the flatter spectra (both in kinetic energy and enstrophy) indicate a submesoscale turbulent eddy activity.

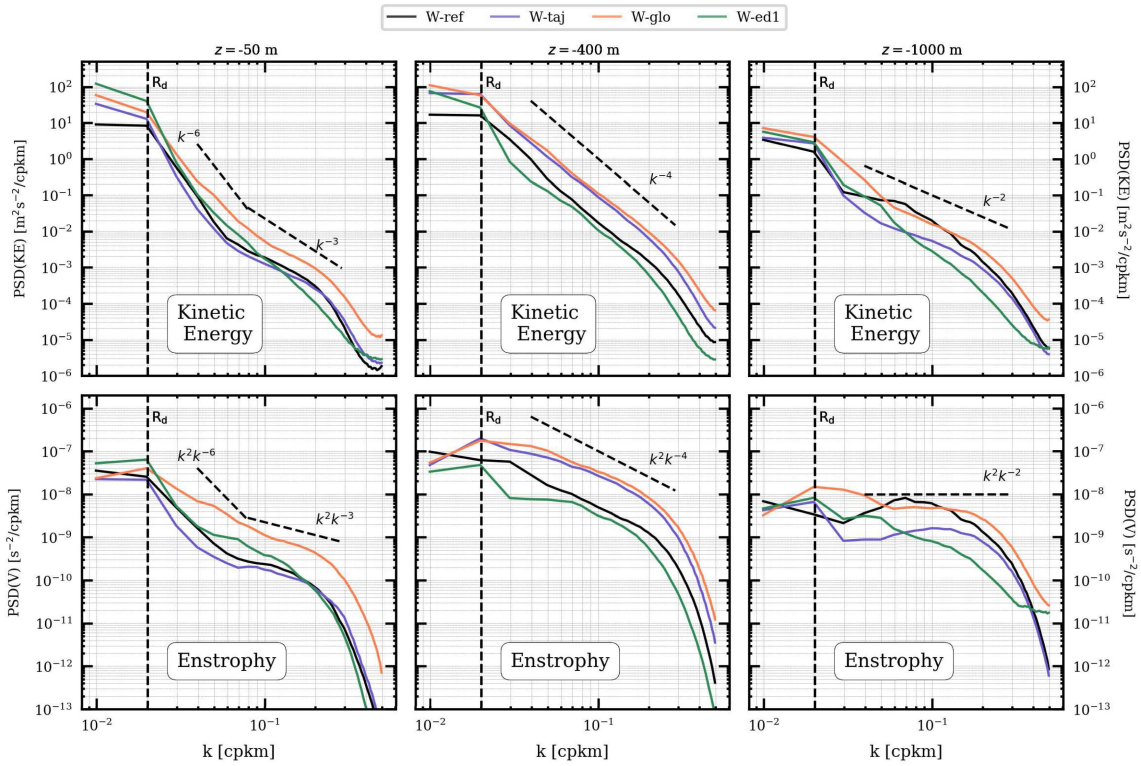

Figure 14. Power Spectrum Density (PSD) of (top) horizontal velocities and (bottom) vorticity averaged from day 100 to day 150 , and computed at three depth levels: (left) near the surface, (middle) at sub-surface, and (right) at depth. The vertical dashed black line indicates the deformation radius (R_d). (Colour online)

3.4. *Impact of surface intensified mesoscale eddies*

To highlight the impact of the surface intensified mesoscale eddies on the BBC water spreading, we compute a dispersion coefficient by following (LaCasce 2008)

$$\kappa = \frac{1}{2}\frac{\mathrm{D}}{\mathrm{D}t}\langle D^2 \rangle , \tag{21}$$

where D is the distance between pairs of particles and $\langle \bullet \rangle$ is the ensemble average over all the pairs of particles. The time evolution of $\langle D^2 \rangle$ is shown in figure 15 (left). In the presence of mesoscale eddies, the distance between pairs of particles increases linearly leading to a dispersion coefficient of about $4000\,\mathrm{m^2\,s^{-1}}$ (cf W-ed1 and W-ed2 experiments). Without any mesoscale eddies initially, the distance between pairs of particles increases abruptly during the 60 first days of the experiment. The corresponding dispersion coefficient is about $9000\,\mathrm{m^2\,s^{-1}}$. Then, the distance between pairs of particles does not evolve anymore and reaches a constant value until the end of the experiment. Indeed, without any mesoscale eddy initially, particles flow in the semi-enclosed basin by following the trajectory of the BBC. As soon as particles reach the Cape of Berbera, they are mainly trapped into the anticyclone created at the Cape of Berbera resulting in the weak dispersion of particles during the last days of the experiment (see figure 15, right, the blue curve). On the contrary, in the W-ed1 and the W-ed2 experiments, particles travel mainly at the periphery of the initial mesoscale eddies (see figure 15, left, the green and orange curves).

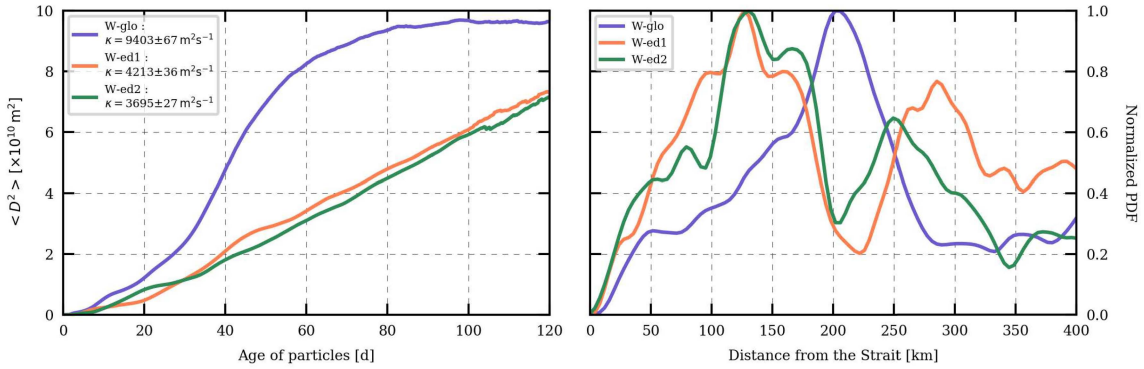

Figure 15. (left) Time evolution of the dispersion $< D^2 >$ computed for the W-glo, the W-ed1 and the W-ed2 experiments. The dispersion coefficients are indicated in the grey box. (right) Normalized PDF of the distance from the Strait of particles being 100 days old computed for the W-glo, the W-ed1 and the W-ed2 experiments. (Colour online)

3.5. *Influence of the seasonality*

As mentioned by Bower *et al.* (2000), the characteristics of the RSW outflow vary depending on the season. The experiments used so far are performed with the winter RSW outflow characteristics. Now we study the impact of this variability on the dynamics in the semi-enclosed basin by setting the salinity and temperature anomalies as well as the thickness of the overflow (see Table 1) to the values found in Bower *et al.* (2000) for summer. The PSD of salinity and vorticity computed at 300 m depth are shown in figure 16a. The magnitude of the PSD of salinity and vorticity are about twice as large in winter as in summer. The shape and slope of salinity spectra are similar regardless the season. This is also true for the PSD of vorticity except at scales comparable to the deformation radius. This indicates that, in summer, the BBC is still unstable, and generates submesoscale eddies rather than mesoscale and submesoscale eddies as in winter. This is related to the thickness of the overflow which is twice as small in summer as in winter. Then, this affects the salt transport through the basin. The transports of salt are shown in figure 16b. In winter (left panel), we observe the impact of the mesoscale dipole cyclone/anticyclone on the salt transport. From the Hovmöller diagram, we estimate that the speed of the salt advection about $20\,\mathrm{km\,d^{-1}} \sim 0.23\,\mathrm{m\,s^{-1}}$ in winter which corresponds to the azimuthal velocity of the mesoscale dipole cyclone/anticyclone. In summer, we estimate the advection speed about $0.02\,\mathrm{m\,s^{-1}}$ resulting in the submesoscale eddies advection.

4. Discussion and Argo floats analysis

To discuss the results of these idealized simulations, we study the data provided by three Argo floats released in the rift of Tadjurah,on the 3$^{\mathrm{rd}}$ of March 2019 by the French Navy (SHOM). The cycle time of Argo floats was set to 48 hours in order to sample well the RSW outflow. The trajectories of Argo floats, and the vertical sections of temperature, salinity, and density collected by the Argo floats, are shown in figure 17.

Though the three Argo floats were launched at close locations, within a short time span, their fates are different. In particular after approximately 180 days, the Argo floats where positioned far from each other (see black dotes in figure 17 (1$^{\mathrm{st}}$ row)). While, float #6902946 is going back toward the rift of Tadjurah, the trajectory of float #6902947 shows two loops that occur upstream and downstream of a cape, while float #6902948 is advected offshore, downstream of the Cape of Berbera. Nonetheless, the three trajectories show that the Argo

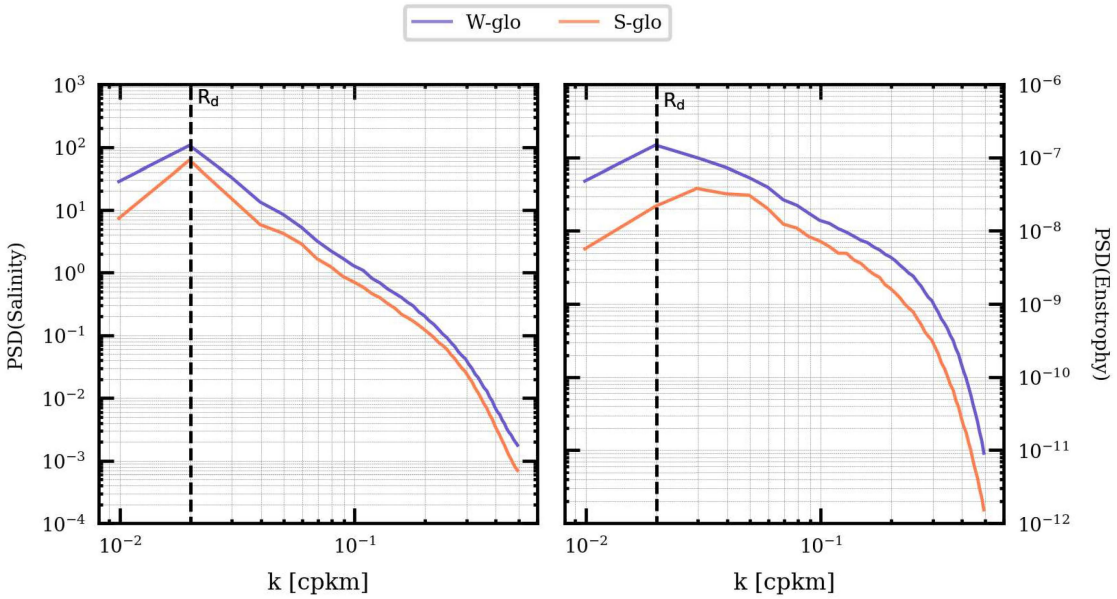

(a)

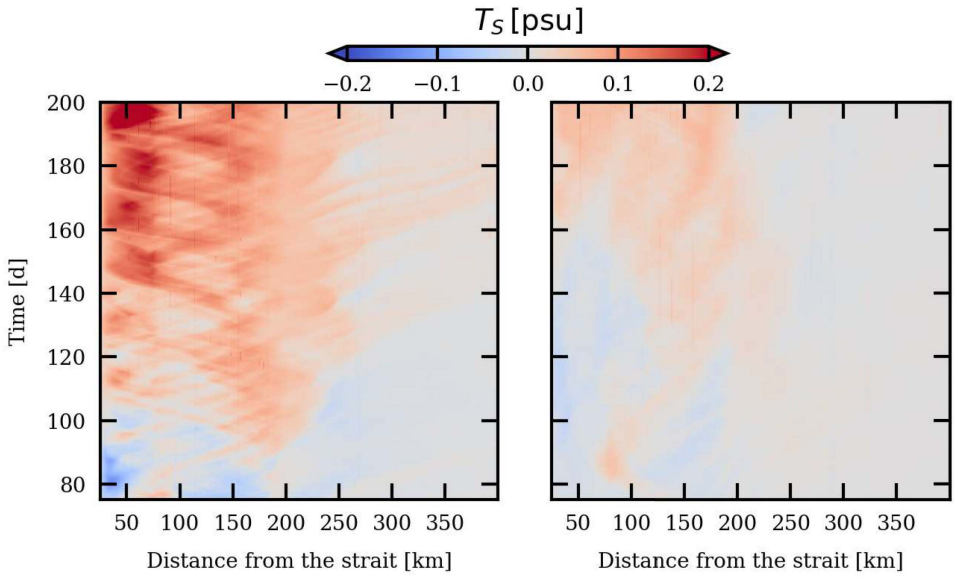

(b)

Figure 16. (a) Power Spectrum Density of (left) salinity and (right) vorticity averaged over 50 days and computed at 300 m depth. (b) Hovmoller diagram of the salinity transport anomaly (left) in winter, and (right) in summer, integrated from 200 down to 600 m depth. (Colour online)

floats are advected along the southern coast of the Gulf of Aden, during the first days, as the RSW outflow usually does. This indicates that the RSW outflow behaves then like a density current. Furthermore, the vertical sections of temperature and salinity indicate that mixing is at play from the rift of Tadjurah to about 150 km along the southern coast of the Gulf of Aden (see the blue crosses in figure 17 (1^{st} row)). In the rift of Tadjurah, RSW extends from 200 down to 1000 meters depth (upstream of the vertical blue dashed lines drawn on vertical sections in figure 17). Its salinity (temperature) varies from 37.5 to 39 psu (from 18

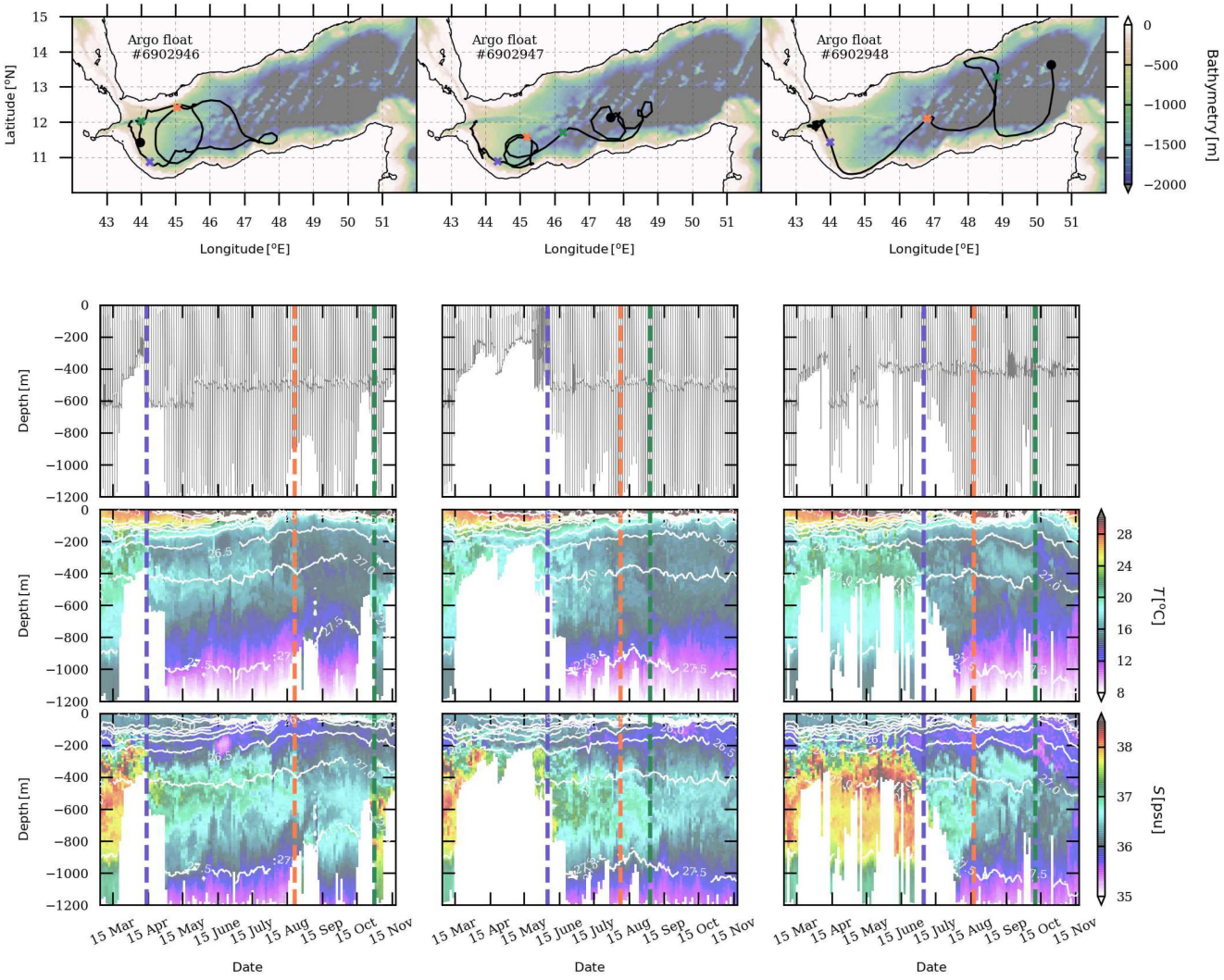

Figure 17. (1st row) Trajectories of the three Argo floats released in the Rift of Tadjurah: (left) #6902946, (center) #6902947, and (right) #6902948. End points are represented in black. The background colors stand for the bathymetry. (2nd row) Time series of the diving depth along the Argo floats trajectories: (left) #6902946, (center) #6902947, and (right) #6902948. (3rd and 4th rows) Vertical sections of temperature and salinity respectively. The density contours are shown in white. The vertical dashed blue (orange,green) lines correspond to the blue (orange,green) crosses represented on the map on the top panels. The end of the trajectories is represented by the points. (Colour online)

to 22°C), corresponding to densities between 26.5 and 27.5 kg m^{-3}. After mixing, the RSW is comprised in a thinner layer between 400 and 600 meters depth, which corresponds to a density layer of approximately 27.25 kg m^{-3} (downstream of the vertical orange dashed lines drawn on middle and bottom panels in figure 17). This is in agreement with the results we obtained with the idealized numerical simulations, corresponding to the vertical mixing stage.

Downstream of the Rift of Tadurah, the parking depths of the three Argo floats are approximately the equilibration depth of the RSW outflow. So, the Argo floats trajectories correspond to their advection by the sub-surface outflow current, between 400 and 600 meters depth (see figure 17 (2nd row)). The time sequences of the Argo floats trajectories are shown in figure 18 with a time windowing of 20 days with the surface geostrophic velocity vectors superimposed (computed from the altimetry).

4.1. *Argo float #6902946*

During the first four months, downstream of the Rift of Tadjurah (from 2019-03-23 to 2019-07-01), the Argo float #6902946 (blue curves in figure 18) is advected along the southern coast of the Gulf of Aden. The salinity and temperature of the RSW outflow decrease little during this period as shown in figure 17 (1$^{\text{st}}$ column). Next, the trajectory of the Argo float #6902946 describes a clockwise loop downstream of the Cape of Berbera (see figure 18 (2$^{\text{nd}}$ row, last column)). We estimate the radius and the azimuthal velocity along the loop curve as

$$R_{\text{loop}} = \frac{1}{2\pi} \sum_{i=1}^{n-1} \Delta L_i \tag{22}$$

and

$$V_{\text{loop}} = \frac{1}{(n-1)\Delta T} \sum_{i=1}^{n-1} \Delta L_i \,, \tag{23}$$

where ΔL_i is the distance between two profiles, ΔT is the cycle time of the Argo float, and n the number of profiles. We obtain $R_{\text{loop}} \sim 23\,\text{km}$ and $V_{\text{loop}} \sim 0.1\,\text{m}\,\text{s}^{-1}$. These estimates suggest that the Argo float sampled a sub-surface submesoscale anticyclonic eddy. Then, the Argo float is advected by a mesoscale anticyclonic eddy toward the northern coast of the Gulf of Aden as shown in figure 18 (3$^{\text{nd}}$ row, 1$^{\text{st}}$ column). The trajectory of the Argo float is finally driven by the mesoscale cyclonic eddy located in the western part of the Gulf of Aden.
These observations support our findings of sub-surface, submesoscale eddies generation at the Cape of Berbera.

4.2. *Argo float #6902947*

The Argo float #6902947 (orange curves in figure 18) follows the southern coast of the Gulf of Aden in the same manner as Argo float #6902946, during the first three months of diving downstream of the Rift of Tadjurah (from 2019-03-23 to 2019-06-11). During this period, the same remarks as above can be made regarding the vertical structure of the water column. Next, upstream of the Cape of Berbera, Argo float #6902947 experiences a anti-clockwise loop-shaped trajectory as shown in figure 18, starting from 2019-06-11 (2$^{\text{nd}}$ row, 2$^{\text{nd}}$ column) to 2019-08-30 (3$^{\text{rd}}$ row, 2$^{\text{nd}}$ column). We estimate the radius and the azimuthal velocity along the loop-shaped trajectory as previously, and we obtain: $R_{\text{loop}} \sim 45\,\text{km}$ and $V_{\text{loop}} \sim 0.1\,\text{m}\,\text{s}^{-1}$. These estimates corroborate the previous results from the numerical simulations suggesting that a sub-surface mesoscale dipole cyclone/anticyclone is generated *via* baroclinic instability upstream of Cape of Berbera. The Argo float #6902947 may have sampled the cyclonic (western) part of the dipole cyclone/anticyclone. Then, the Argo float #6902947 is back on course along the southern coast of the Gulf of Aden. But after 1 month, it is trapped in a sub-surface submesoscale anticyclonic eddy downstream of the Cape of Berbera as shown in figure 18 from 2019-09-19 (4$^{\text{th}}$ row, 1$^{\text{st}}$ column) to 2019-11-18 (4$^{\text{th}}$ row, 3$^{\text{rd}}$ column). This suggests that sub-surface submesoscale anticyclonic eddies form downstream of the Cape of Berbera in agreement with the results from the numerical experiments.

4.3. *Argo float #6902948*

The Argo float #6902948 (green curves in figure 18) remains blocked in the Rift of Tadjurah for approximatively 5 months sampling its waters, before travelling along the southern coast of the Gulf of Aden as shown in figure 18. Then, at Cape of Berbera, it is expelled from

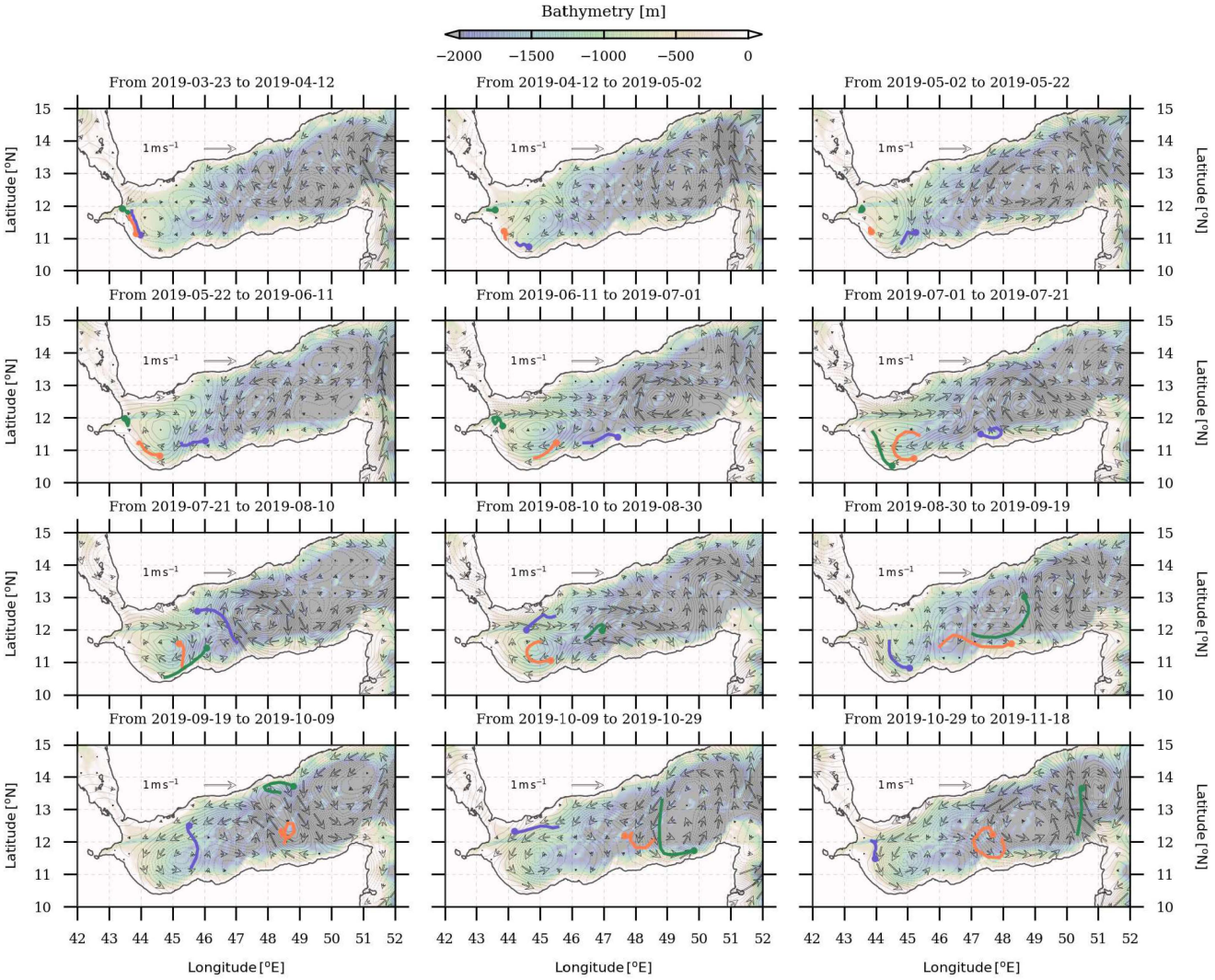

Figure 18. Time sequences of the Argo floats trajectories: (blue) #6902946, (orange) #6902947, and (green) #6902948. The time windowing is 20 days; the dates are indicated above panels. The arrows stand for the geostrophic velocity vectors computed from the altimetry at the day corresponding to the half of the time windowing. Absolute dynamic bathymetry anomalies contours are drawn in (positive values) solid and (negative values) dashed black. The background colors stand for the bathymetry. (Colour online)

the coast toward the center of the gulf (as in the numerical experiments). The trajectory of the Argo float #6902948 is finally driven by the mesoscale eddies that dominate the surface circulation down to about 1000 meters depth especially in the eastern part of the Gulf of Aden (Morvan *et al.* 2020).

5. Conclusion

We studied the dynamics of a bottom buoyant current flowing into a semi-enclosed basin by setting and analyzing idealized numerical simulations performed with a primitive equation model. We showed that the bottom buoyant current adjusts vertically, and experiences vertical mixing. The vertical mixing is stronger in the presence of the rift of Tadjurah due to the vertical velocity induced by the curvature of the isobaths. Subsequently horizontal mixing occurs as the BBC flows over the southern continental slope. There, a standing dipole

cyclone/anticyclone vortex is generated tvia baroclinic instability. Submesoscale eddies are also generated via horizontal shear instability of the bottom frictional boundary layer. Submesoscale eddies accumulate downstream of the Cape of Berbera, and participate to the sustainability of the anticyclonic part of the dipole cyclone/anticyclone. We also show that the rows of mesoscale eddies initially implemented in the flow, have an impact on the dispersion of the bottom buoyant current water. Without any initial mesoscale eddies, the bottom buoyant current water is mostly advected in the anticyclone standing downstream of the Cape of Berbera, while in the presence of initial mesoscale eddies, the bottom buoyant current is advected at the periphery and in the core of them. Finally, the data provided by three Argo floats corroborate the results obtained numerically, in particular the formation of sub-surface submesoscale eddies at capes, and the deep influence of mesoscale eddies.

Data availability

Model outputs are available upon request. Argo floats data are available online at https://fleetmonitoring.euro-argo.eu/dashboard.

Author contributions

MM designed and performed the numerical experiments. MM and XC analysed the results and wrote the manuscript. PLH, CdM, SC, and SL contributed to the writing of the manuscript. XC, SL, SC, PLH, CdM and MM contributed to the Argo floats deployment program.

Disclosure statement

No potential conflict of interest was reported by the authors.

Acknowledgements

We acknowledge support from UBO and SHOM. The simulations were performed using the HPC resources from DATARMOR of "Pôle de Calcul Intensif pour la Mer" at Ifremer, Brest, France.

References

Aiki, H., Takahashi, K. and Yamagata, T., The Red Sea outflow regulated by the Indian monsoon. *Cont. Shelf Res.*, 2006, **26**, 1448–1468.

Al Saafani, M., Shenoi, S., Shankar, D., Aparna, M., Kurian, J., Durand, F. and Vinayachandran, P., Westward movement of eddies into the Gulf of Aden from the Arabian Sea. *J. Geophys. Res.-Oceans*, 2007, **112**, 1–12.

Blanke, B. and Raynaud, S., Kinematics of the Pacific equatorial undercurrent: An Eulerian and Lagrangian approach from GCM results. *J. Phys. Oceanogr.*, 1997, **27**, 1038–1053.

Bower, A.S., Fratantoni, D.M., Johns, W.E. and Peters, H., Gulf of Aden eddies and their impact on Red Sea Water. *Geophys. Res. Lett.*, 2002, **29**, 21–1.

Bower, A.S. and Furey, H.H., Mesoscale eddies in the Gulf of Aden and their impact on the spreading of Red Sea Outflow Water. *Prog. Oceanogr.*, 2012, **96**, 14–39.

Bower, A.S., Hunt, H.D. and Price, J.F., Character and dynamics of the Red Sea and Persian Gulf outflows. *J. Geophys. Res.-Oceans*, 2000, **105**, 6387–6414.

Bower, A.S., Johns, W.E., Fratantoni, D.M. and Peters, H., Equilibration and circulation of Red Sea Outflow Water in the western Gulf of Aden. *J. Phys. Oceanogr.*, 2005, **35**, 1963–1985.

Charney, J.G. and Stern, M., On the stability of internal baroclinic jets in a rotating atmosphere. *J. Atmos. Sci.*, 1962, **19**, 159–172.

Ciani, D., Carton, X. and Verron, J., On the merger of subsurface isolated vortices. *Geophys. Astrophys. Fluid Dyn.*, 2016, **110**, 23–49.

Gula, J., Molemaker, M.J. and McWilliams, J.C., Gulf Stream dynamics along the southeastern US seaboard. *J. Phys. Oceanogr.*, 2015, **45**, 690–715.

Gula, J., Molemaker, M.J. and McWilliams, J.C., Topographic generation of submesoscale centrifugal instability and energy dissipation. *Nat. Commun*, 2016, **7**, 12811.

Ilıcak, M., Özgökmen, T.M. and Johns, W.E., How does the Red Sea outflow water interact with Gulf of Aden Eddies?. *Ocean Model.*, 2011, **36**, 133–148.

LaCasce, J., Statistics from Lagrangian observations. *Prog. Oceanogr.*, 2008, **77**, 1–29.

Large, W.G., McWilliams, J.C. and Doney, S.C., Oceanic vertical mixing: A review and a model with a nonlocal boundary layer parameterization. *Rev. Geophys.*, 1994, **32**, 363–403.

L'Hégaret, P., de Marez, C., Morvan, M., Meunier, T. and Carton, X., Spreading and vertical structure of the Persian Gulf and Red Sea outflows in the northwestern Indian Ocean. *J. Geophys. Res.-Oceans*, 2020, **(submitted)**.

Morvan, M., L'Hégaret, P., Carton, X., Gula, J., Vic, C., Marez, C.d., Sokolovskiy, M. and Koshel, K., The life cycle of submesoscale ?ddies generated by topographic interactions. *Ocean Sci.*, 2019, **15**, 1531–1543.

Morvan, M., L'Hégaret, P., de Marez, C., Carton, X., Corréard, S. and Baraille, R., Life cycle of mesoscale eddies in the Gulf of Aden. *Geophys. Astrophys. Fluid Dyn.*, 2020, pp. 1–19.

Murray, S.P. and Johns, W., Direct observations of seasonal exchange through the Bab el Mandab Strait. *Geophys. Res. Lett.*, 1997, **24**, 2557–2560.

Nof, D., Paldor, N. and Van Gorder, S., The reddy maker. *Deep-Sea Res. Pt. I*, 2002, **49**, 1531–1549.

Shchepetkin, A.F. and McWilliams, J.C., The regional oceanic modeling system (ROMS): a split-explicit, free-surface, topography-following-coordinate oceanic model. *Ocean Model.*, 2005, **9**, 347–404.

Shi, C. and Nof, D., The destruction of lenses and generation of wodons. *J. Phys. Oceanogr.*, 1994, **24**, 1120–1136.

Smeed, D.A., Exchange through the Bab el Mandab. *Deep-Sea Res. Pt. II*, 2004, **51**, 455–474.

von Karman, T., Gottingen Nachrichten. *Math. Phys. Kl*, 1912, **13**, 547.